Aspects of the Reaction Mechanism of Ethane Combustion. Conformations of the Ethylperoxy Radical

Geoffrey E. Quelch,† Mary M. Gallo,# and Henry F. Schaefer III*

Contribution from the Center for Computational Quantum Chemistry, University of Georgia, Athens, Georgia 30602. *Received February 6, 1992*

Abstract: The detailed molecular understanding of hydrocarbon combustion processes is recognized as an important goal. The specific system studied—via ab initio theoretical methods—in this work is the reaction between the ethyl radical (C_2H_5•) and molecular oxygen (O_2). It may be argued that further experimental work on this system will yield limited new insights until theoretical investigations of the potential energy surface are made. Theoretical methods used include self-consistent-field (SCF) and configuration interaction including all single and double excitations (CISD) with up to double zeta plus polarization (DZP) quality basis sets. A total of 55 distinct stationary points on the $C_2H_5O_2$• potential energy surface were considered here. Two excited states of the ethylperoxy radical, six conformers of the ground $^2A''$ state, and four conformers of the excited $^2A'$, state were studied. For the ground-state surface, the barrier between the staggered and gauche structures is only 1.0 kcal mol^{-1}. The barrier to internal rotation of the methyl group is between 2.5 and 3.0 kcal mol^{-1} depending on the level of theory.

I. Introduction

The understanding of the combustion reactions of hydrocarbons, most specifically alkanes, is an important scientific goal.[1-17] The system under study in the present work is the reaction of the ethyl radical with molecular oxygen. This system has been studied extensively with experimental methods; previous work will be reviewed briefly, and more detailed information may be found in refs 18-32.

Important early work on low-temperature alkane combustion was performed by Knox[6] and Benson.[18] A good summary, by Benson, is given in ref 10. This initial research is still the basis for more modern interpretations.[2] Benson particularly, through tabulations of thermochemical quantities and additivity rules for molecular properties,[7] has provided much insight.

Alkane combustion is initiated by abstraction of a hydrogen atom from the alkane (RH) by an oxygen molecule to form the alkyl radical (R•). At temperatures below 500 K this radical reacts further with O_2 to form the alkylperoxy radical RO_2• reversibly:

$$R^\bullet + O_2 \rightleftarrows RO_2^\bullet \quad (1)$$

At higher temperatures (>600 K) the reaction can be represented by:

$$R^\bullet + O_2^\bullet \rightarrow R_{-H} + HO_2^\bullet \quad (2)$$

where R_{-H} is the alkene (the dehydrogenated alkyl radical). Reaction 2 is the representation of a global change which may or may not proceed directly from reactants to products.

According to Benson,[18] the rate of reaction for alkane combustion was essentially independent of the specific alkane used. This leads to the use of ethane as a "model" alkane since its secondary reactions are less complex due to the size of the molecule (i.e., only two carbon atoms). Other observations[33] showed that (1) is a fast bimolecular reaction compared to the competing reactions of R• and that RO_2• decomposition is a rapid unimolecular process.

Two early explanations were offered to account for this change in mechanism or "turnover". The first[6,18] assumes an effective activation energy for process 2 of 5-10 kcal mol^{-1};[28] this value is required to provide the turnover. Knox[6] and Benson[18] used (1) and (2) to construct models of combustion that could explain the observed changes in rate constant and product yields. These models, due to the global nature of (2), are independent of any intermediates in the reaction and thus have been widely used. The second explanation for the turnover in the reaction assumes a second decomposition pathway for RO_2•.[4,5,8] This pathway is the basis for the modern interpretation and is discussed more fully below.

There is much evidence to support the product determination

† Present address: Department of Chemistry, P.O. Box 7486, Wake Forest University, Winston-Salem, NC 27109.

Present address: BIOSYM, 10065 Barnes Canyon Rd., San Diego, CA 92121.

(1) Minkoff, G. J.; Tipper, C. F. H. *Chemistry of Combustion Reactions*; Butterworths: London, 1962.
(2) *Combustion Chemistry*; Gardiner, W. C., Ed.; Springer-Verlag: New York, 1985.
(3) Hucknall, K. J. *Chemistry of Hydrocarbon Combustion*; Chapman and Hall: New York, 1985.
(4) Pollard, R. T. In *Comprehensive Chemical Kinetics*; Bamford, C. H., Tipper, C. F. H., Eds.; Elsevier: New York 1977; Vol. 17, pp 249-367.
(5) McKay, G. *Prog. Energy Combust. Sci.* **1977**, *3*, 105.
(6) Knox, J. H. *Combust. Flame* **1965**, *9*, 297.
(7) Benson, S. W. *Thermochemical Kinetics*; John Wiley: New York, 1976.
(8) Fish, A. *Angew. Chem., Int. Ed. Engl.* **1968**, *7*, 45.
(9) Baker, R. R.; Baldwin, R. R.; Walker, R. W. *J. Chem. Soc., Faraday Trans. 1* **1975**, *71*, 756.
(10) Benson, S. W.; Nangia, P. S. *Acc. Chem. Res.* **1979**, *12*, 223.
(11) Baldwin, R. R.; Bennett, J. P.; Walker, R. W. *J. Chem. Soc., Faraday Trans. 1* **1980**, *76*, 1075.
(12) Lenhardt, T. M.; McDade, C. E.; Bayes, K. D. *J. Chem. Phys.* **1980**, *72*, 304.
(13) Ruiz, R. P.; Bayes, K. D. *J. Phys. Chem.* **1984**, *88*, 2592.
(14) Cox, R. A.; Cole, J. A. *Combust. Flame*, **1985**, *60*, 109.
(15) Gulati, S. K.; Mather, S.; Walker, R. W. *J. Chem. Soc., Faraday Trans. 2* **1987**, *83*, 2171.
(16) Gulati, S. K.; Walker, R. W. *J. Chem. Soc., Faraday Trans. 2* **1988**, *84*, 401.
(17) Stothard, N. D.; Walker, R. W. *J. Chem. Soc., Faraday Trans.* **1990**, *86*, 2115.
(18) Benson, S. W. *J. Am. Chem. Soc.* **1965**, *87*, 972.
(19) Baldwin, R. R.; Pickering, I. A.; Walker, R. W. *J. Chem. Soc., Faraday Trans. 1* **1980**, *76*, 2374.
(20) Plumb, I. C.; Ryan, K. R. *Int. J. Chem. Kinet.* **1981**, *13*, 1011.
(21) Slagle, I. R.; Feng, Q.; Gutman, D. *J. Phys. Chem.* **1984**, *88*, 3648.
(22) Slagle, I. R.; Ratajczak, E.; Gutman, D. *J. Phys. Chem.* **1986**, *90*, 402.
(23) Baldwin, R. R.; Dean, C. E.; Walker, R. W. *J. Chem. Soc., Faraday Trans. 2* **1986**, *82*, 1445.
(24) McAdam, K. G.; Walker, R. W. *J. Chem. Soc., Faraday Trans. 2* **1987**, *83*, 1509.
(25) Kaiser, E. W.; Rimai, L.; Wallington, T. J. *J. Phys. Chem.* **1989**, *93*, 4094.
(26) Wallington, T. J.; Andino, J. M.; Kaiser, E. W.; Japar, S. M. *Int. J. Chem. Kinet.* **1989**, *21*, 1113.
(27) Kaiser, E. W.; Wallington, T. J.; Andino, J. M. *Chem. Phys. Lett.* **1990**, *168*, 309.
(28) Wagner, A. F.; Slagle, I. R.; Sarzynski, D.; Gutman, D. *J. Phys. Chem.* **1990**, *94*, 1853.
(29) Bozzelli, J. W.; Dean, A. M. *J. Phys. Chem.* **1990**, *94*, 3313.
(30) Kaiser, E. W.; Lorkovic, I. M.; Wallington, T. J. *J. Phys. Chem.* **1990**, *94*, 3352.
(31) Dagaut, P.; Cathonnet, M.; Boettner, J.-C. *Int. J. Chem. Kinet.* **1991**, *23*, 437.
(32) Baldwin, R. R.; Stout, D. R.; Walker, R. W. *J. Chem. Soc., Faraday Trans.* **1991**, *87*, 2147.
(33) Dingleday, D. P.; Calvert, J. G. *J. Am. Chem. Soc.* **1963**, *85*, 856. Calvert, J. G.; Sleepy, W. C. *Ibid.* **1959**, *81*, 769.

0002-7863/92/1514-8239$03.00/0

steps in hydrocarbon oxidation. All evidence shows that, at high temperatures, the initial products of the reactions are alkenes; ethane is again the "model" alkane since it is the smallest alkane for which a turnover in mechanism is possible.

More recent work on alkane combustion by Walker and coworkers[9,19] has shown that the alkene is formed from the conjugate alkane (RH) either in a direct $R^{\bullet} + O_2$ step or possibly via $RO_2^{\bullet}$ radicals by an internal hydrogen atom transfer. However, under the conditions of the experiments (essentially due to the equilibrated nature of reaction 1), it was impossible to distinguish between the two pathways. The possibility of formation of the alkene from the decomposition of an $R_{-H}O_2H$ species was ruled out. The authors suggest, however, that O-hetero products are formed from the peroxy radical via the elementary reaction

$$RO_2^{\bullet} \rightarrow R_{-H}O_2H \qquad (3)$$

that is, an internal hydrogen abstraction followed by the elimination of OH.

$$R_{-H}O_2H \rightarrow R_{-H}O^{\bullet} + OH \qquad (4)$$

In 1981, Plumb and Ryan[20] published an important study of the ethyl radical reaction with oxygen at room temperature (298 K). They measured the branching ratio between reactions 5 and 6:

$$C_2H_5^{\bullet} + O_2 + M \rightarrow C_2H_5O_2^{\bullet} + M \qquad (5)$$

$$C_2H_5^{\bullet} + O_2 \rightarrow C_2H_4 + HO_2^{\bullet} \qquad (6)$$

where (5) is an elementary reaction and (6) may be a direct or a multistep process. The results of their work showed that the percentage of $C_2H_5^{\bullet}$ removed via (6) was between 6 and 15.4% of the total reduction in $C_2H_5^{\bullet}$ within the range of pressures studied. The larger percentage occurred at the lower pressure in the reaction system. Plumb and Ryan's work also showed that the total rate coefficient for $C_2H_5^{\bullet} + O_2 \rightarrow$ products increased with increase in pressure and exhibited a high-pressure limiting value. In conclusion, Plumb and Ryan state that the reaction $C_2H_5^{\bullet} + O_2 \rightarrow$ products must be a combination of two parallel processes, reactions 5 and 6, having different responses to pressure since the reaction has a nonzero high-pressure limiting rate coefficient. The first (eq 5) proceeds through a long-lived complex to produce $C_2H_5O_2^{\bullet}$ and is highly pressure dependent; the second (eq 6) is a direct mechanism, independent of gas density, and produces C_2H_4 as its ultimate product.

Slagle, Feng, and Gutman,[21] in a 1984 paper, summarized the work to date. At temperatures above 580 K, the equilibrium of reaction 1 is far to the left at the usual pressures of O_2 as observed by Knox and Benson;[6,18] however, product yields in this temperature regime reveal that almost complete conversion of $R^{\bullet}$ to the corresponding R_{-H} has occurred. Two possibilities have been proposed to explain this.

(A) Parallel, Uncoupled Reactive Scheme. This is essentially the global change described by (2) with an activation energy of 5–10 kcal mol^{-1},[7] occurring in parallel with the elementary reaction 1. The former reaction becomes more important as the temperature increases due to the increased rate constant with rising temperature and also the shift in the $R^{\bullet}$ to $RO_2^{\bullet}$ in equilibrium 1.

(B) Coupled Reactive Paths. This path results from a second decomposition channel of $RO_2^{\bullet}$ proposed earlier,[4,5,8] namely:

$$R^{\bullet} + O_2 \rightleftarrows RO_2^{\bullet} \rightarrow R_{-H} + HO_2^{\bullet} \qquad (7a,b)$$

where, again, (7b) is probably a multistep process. The minor importance of (7b) at ambient temperature is due to the stability of $RO_2^{\bullet}$. Decomposition of $RO_2^{\bullet}$ to $R_{-H} + HO_2^{\bullet}$ is never rapid compared to the reverse reaction. At low enough pressure (≈10 Torr[20,26,27,30]), reaction 7 can proceed almost completely to products. The coupled reactive path can, however, account for the increased importance of alkene production (as a fraction of the $R^{\bullet} + O_2$ encounters that produce products). Mechanism B is consistent with the product yield and rate constant determination of Baldwin et al. at 750 K.[19]

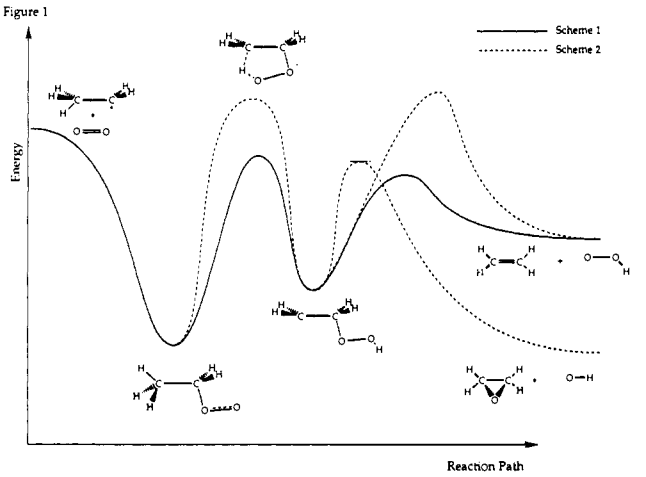

Figure 1. A comparison of potential energy surfaces for the $C_2H_5^{\bullet} + O_2$ reaction. The figure is schematic only. Comparisons of energy differences are presented in the tables and discussed in the text.

The results of the work by Slagle, Feng, and Gutman[21] on the temperature dependence of the reaction between $C_2H_5^{\bullet}$ and O_2 showed that mechanism B can easily account for the observed features of the ethane combustion reaction. This conclusion is also reached from a more recent study by Wallington and coworkers.[26,30] However, the work of Plumb and Ryan, as described above, is incompatible with mechanism B since they found that reaction 6 has a high-pressure limiting rate constant. If this is true, all the $C_2H_5O_2^{\bullet}$ will be collision stabilized and therefore none will be available to yield C_2H_4. This can easily be explained by mechanism A.

Slagle et al.[21] have proposed a semiquantitative potential energy surface to account for the results they obtained; this surface is given in Figure 1 as the solid line. The reaction proceeds by barrierless addition of O_2 to the ethyl radical to form the ethylperoxy radical, which then rearranges to give a five-membered ring transition state for the transfer of a hydrogen atom. Subsequent to this, the reaction proceeds through the ethylhydroperoxy intermediate and moves to products ($C_2H_4 + HO_2^{\bullet}$) through another transition state.

One aspect of the $C_2H_5^{\bullet} + O_2$ surface that has received attention is the role of $C_2H_4O_2H$, the ethylhydroperoxy radical—if indeed it is relevant at all—in the overall scheme. Baldwin, Dean, and Walker[23] have studied the reaction of $HO_2^{\bullet}$ with C_2H_4 and have postulated that C_2H_4O is formed in two steps:

$$HO_2^{\bullet} + C_2H_4 \xrightarrow{a} C_2H_4O_2H \xrightarrow{b} C_2H_4O + OH^{\bullet} \qquad (8a,b)$$

Experimental evidence quoted by Walker et al.[23] also indicates that the $C_2H_4O_2H$ species does not decompose to any great extent to the alkene and $HO_2^{\bullet}$.

This discussion has obvious repercussions for the mechanism favored in the work of Slagle et al.[21] As mentioned previously,[21] the $C_2H_5^{\bullet}$ and $C_2H_5O_2^{\bullet}$ species are in equilibrium so that kinetic differentiation between the direct one-step production of C_2H_4 and $HO_2^{\bullet}$ by reaction 6 or the decomposition of $C_2H_5O_2^{\bullet}$ by the possibly multistep reaction 7b cannot be made within the temperature range studied (650–770 K). In order to reconcile this fact with the model proposed by Slagle et al.,[21] Walker et al.[23] suggest the following three modifications to the surface of Slagle et al.: (1) an increase in the height of the second transition state barrier; (2) a second decomposition channel for the ethylhydroperoxy radical to oxirane and OH; and (3) an increase in the barrier height of the first transition state. This revised potential energy surface is given as the broken line in Figure 1.

Unfortunately, one consequence of these changes is that it is no longer possible to explain the negative temperature coefficient of the overall process 6 as found by Slagle et al.[21] As an alternative, Walker et al. suggest that the reaction does not pass through the ethylhydroperoxy radical intermediate ($C_2H_4O_2H$). This interpretation has received further support in more recent

work.[24] The possibility of a concerted process to form ethene was suggested:

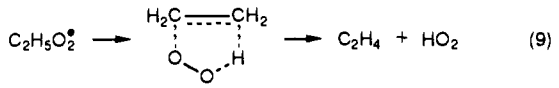

(9)

The result of this modification, assuming the barrier to the formation of this transition state is lower than that of the back reaction, is that Slagle et al.'s explanation of the temperature effect would still be valid and the overall mechanism also would be able to explain the pressure effect.

More recent work by McAdam and Walker[24] has confirmed the negative temperature coefficient found by Slagle et al;[21] McAdam and Walker's results, when extrapolated to 295 K, yield good agreement (within 10%) with the work of Plumb and Ryan[20] but with a considerable uncertainty. McAdam and Walker[24] then suggest that the agreement between their extrapolated results and Plumb and Ryan's results is a good indicator that C_2H_4 is formed by the same mechanism at all temperatures and that this mechanism must differ from all previously postulated mechanisms. The direct decomposition of the ethylperoxy radical to form C_2H_4 is consistent with the high-temperature results of Walker and Slagle but not with the room-temperature results of Plumb and Ryan.[20] With the $C_2H_4O_2H$ intermediate ruled out by this and previous work[9,23] (and the direct bimolecular reaction 6 producing products in a one-step process being ruled out by the negative temperature coefficient), the authors suggest that the formation of a long-lived cyclic intermediate is the best explanation. This intermediate is suggested to arise as a consequence of the unique diradical nature of the O_2 moiety.

Later work by Wallington and co-workers[25-27,30] on the pressure dependence of (6) at room temperature has shown conclusively that the C_2H_4 yield at high pressure goes essentially to zero, contradicting previous work by Plumb and Ryan[20] who found a nonzero high-pressure limit. This result essentially shows that there is no parallel uncoupled route at low temperature. All the C_2H_4 is therefore formed from the decomposition of $C_2H_5O_2^{\bullet}$, and at high pressure this species is completely deactivated by collisions, preventing further reaction to C_2H_4.

There were several papers published on the ethyl radical system in 1990, the most extensive of which was by Wagner, Slagle, Sarzynski, and Gutman.[28] This work is a combined theoretical and experimental study of this reaction system. In brief, the authors have devised a theoretical model (based on the semiquantitative potential energy surface given by Slagle et al.[21]) that satisfactorily accounts for all the experimental observations for the system, namely, temperature and pressure dependence, magnitude and temperature dependence of the equilibrium 1, and the temperature and density dependence of the C_2H_4 branching ratios. The success of the model is interpreted as strong evidence that the addition mechanism is dominant up to 1000 K, while the direct abstraction mechanism will be increasingly important at temperatures >1000 K.

A subsequent paper by Bozzelli and Dean,[29] also using a theoretical kinetics model, was published soon after the Wagner paper. Whereas Wagner et al.[28] used RRKM methods for their model, Bozzelli and Dean used an alternative scheme, the QRRK[34] method. The conclusion they draw from this alternative theoretical approach is that the direct H-transfer reaction is unimportant at lower temperatures. The RO_2H intermediate, if formed, dissociates almost completely to $C_2H_4 + HO_2^{\bullet}$ at low pressures. At higher pressures, a larger fraction of this intermediate can be stabilized; however, this potential well is shallow, leading essentially to complete conversion to $C_2H_4 + HO_2^{\bullet}$ at high temperature. This work also confirms assumptions made by Wagner concerning the barrier height of the second transition state, and disagrees with values given by Baldwin et al.[23] and Gulati et al.[15] Bozzelli and Dean[29] suggest that the oxirane production that is observed may be a complication resulting in side reactions involving atomic oxygen due possibly to the fact that in Walker's experiment the $HO_2^{\bullet}$ remains in the reaction vessel longer. Therefore, it is concluded that the oxirane production channel is not a genuine part of the pathway to formation of ethene. The authors state: "We caution that accurate thermodynamic parameters *must* be used in addition to correct bi- and unimolecular rate constants for the analysis to be meaningful."

Further support for the work of Wagner et al. has been published. Kaiser, Lorkovic, and Wallington[30] have reported work investigating the pressure dependence of the C_2H_4 yield for the reaction. Their experiments show that the pressure dependence is close to that predicted in the model derived by Wagner.

II. Ethyl and Ethylperoxy Radicals

The ethyl radical and its reactions with species other than O_2 have been studied extensively by experiment. In addition, much theoretical work has been published on the radical. The structure of $C_2H_5^{\bullet}$ was first determined by Pacansky and Dupuis[35] using a valence triple-zeta (TZV) basis set with the restricted Hartree–Fock (RHF) level of theory and TZV plus polarization functions (TZVp) with UHF level studies. The optimized geometries for these two methods were similar. The barrier to internal rotation about the C–C bond was found to be small (0.2 kcal mol^{-1} at RHF/TZV, 0.06 kcal mol^{-1} at UHF/TZV, and 0.16 kcal mol^{-1} at UHF/TZVp). Subsequently, Pacansky and Dupuis,[36] using experimental data and theoretical studies, made the first assignment of the infrared (IR) spectrum of the ethyl radical. The IR spectrum has subsequently been reported by other groups.[37] Very recently, new studies on the IR and Raman spectra also have been published,[38] along with theoretical studies at up to the UMP2/6-311G** level of theory. Three-dimensional molecular orbital (MO) plots have shown that the highest occupied MO (HOMO) of the ethyl radical contains contributions from the C2p radical site and also from the βCH bond orbital.

Theoretical investigations also have been reported concerning the ultraviolet (UV) absorption spectrum of the ethyl radical,[39,40] with experimental work being published simultaneously.[41] These studies showed that the lowest-lying excited states are Rydberg in nature. In addition, multiconfiguration self-consistent field (MCSCF) and configuration interaction (CI) work showed that once excitation to the lowest 3p Rydberg state occurs, dissociation proceeds without a barrier to the methyl radical and $^1B_1$ methylene. This observation can account for the continuous nature of the ethyl spectrum. There also is evidence that the equilibrium structure of the 3p Rydberg state is nonclassical in nature; i.e., it contains an H atom in a bridging position.

The barrier to internal rotation has received much attention since the first report of Pacansky and Dupuis. Values reported are 0.07–0.13 kcal mol^{-1} [42] using SCF, fourth-order Møller–Plesset perturbation theory (MP4) and CI with single and double excitations (CISD) methods with 6-31G* and 6-31G** basis sets, and 0.17–0.14 kcal mol^{-1} [43] using up to MP4 and 6-311G** basis sets. Zero-point vibrational energy corrections, however, place the eclipsed form slightly below the staggered form. A further analysis of the zero-point vibrational energy correction to the energy difference has been published.[44] The best result of Pacansky and Dupuis for the barrier is 0.07 kcal mol^{-1}. These investigators note that the barrier may be considered to be vibrationally induced and that the preferred orientation is determined largely by the zero-point vibrational energy.

(34) Dean, A. M. *J. Phys. Chem.* **1985**, *89*, 4600.

(35) Pacansky, J.; Dupuis, M. *J. Chem. Phys.* **1978**, *68*, 4276.
(36) Pacansky, J.; Dupuis, M. *J. Am. Chem. Soc.* **1982**, *104*, 415.
(37) Chettur, G.; Snelson, A. *J. Phys. Chem.* **1987**, *91*, 3483.
(38) Pacansky, J.; Koch, W.; Miller, M. D. *J. Am. Chem. Soc.* **1991**, *113*, 317.
(39) Lengsfield, B. H.; Siegbahn, P. E. M.; Liu, B. *J. Chem. Phys.* **1984**, *81*, 710.
(40) Blomberg, M. R. A.; Liu, B. *J. Chem. Phys.* **1985**, *83*, 3995.
(41) Wendt, H. R.; Hunziker, H. *J. Chem. Phys.* **1984**, *81*, 717.
(42) Peeters, D.; Leroy, G.; Natagne, M. *J. Mol. Struct. (THEOCHEM)* **1988**, *166*, 267.
(43) Wong, M. W.; Baker, J.; Nobes, R. H.; Radom, L. *J. Am. Chem. Soc.* **1987**, *109*, 2245.
(44) Suter, H. U.; Ha, T.-K. *Chem. Phys.* **1991**, *154*, 227.

Table I. Selected Geometric Parameters (Å and deg) for the $^2A''$ State of the Ethylperoxy Radical at the SCF Level of Theory[a]

	[s,s]		[s,e]		[e,s]		[e,e]		[s,g]		[s,sg]		reactants	
	DZ	DZP	DZ	DZP	DZ	DZP	DZ	DZP	DZ	DZP	DZ	DZP	DZ	DZP
r(CC)	1.520	1.516	1.524	1.517	1.531	1.530	1.536	1.532	1.523	1.519	1.522	1.518	1.509	1.503
r(CO)	1.461	1.424	1.472	1.436	1.464	1.428	1.480	1.443	1.461	1.425	1.465	1.429		
r(OO)	1.367	1.305	1.360	1.299	1.366	1.304	1.356	1.295	1.367	1.305	1.363	1.302	1.199	1.166
oop(C_2)	-36.5	-35.6	-40.3	-39.1	-37.2	-36.3	-41.8	-40.5					12.6	18.3
θ(CCO)	106.7	107.5	114.8	115.4	106.9	107.7	116.4	117.0	111.7	112.2	109.2	109.7		
θ(COO)	111.7	111.0	115.5	114.8	111.7	111.0	117.1	116.4	109.7	111.3	113.0	112.6		
Hess. index	0	0	1	1	1	1	2	2	0	0	1	1		

[a] Nomenclature is described in the text. The reactants are $C_2H_5^\bullet$ and O_2. The Hessian index is the number of imaginary frequencies.

The ethylperoxy radical has been studied extensively, particularly in self-reactions. The majority of reports have included the study of the molecule itself so that a specific ethylperoxy radical signature may be followed. In this latter vein, electron spin resonance (ESR) studies have been reported[45-48] as well as UV spectra,[49-52] IR observations,[53,54] and molecular modulation spectra.[55]

Several theoretical studies have been published on the ethylperoxy radical. Early work employed the semiempirical methods SCF-INDO[56-58] and MINDO/2'.[59] Two recent papers have used ab initio molecular orbital theory,[60,61] both of which use unrestricted Hartree–Fock (UHF) and unrestricted Møller–Plesset perturbation theory at second-order (UMP2) methods with 6-31G* and 6-311G** basis sets. The work by Skancke and Skancke contains some studies using UMP4 theory, but the authors investigated only the global minimum of the ethylperoxy radical (assumed to be the trans C–C–O–O conformer), whereas Boyd et al. studied both cis and trans conformers. Neither paper examines the gauche structure. Boyd et al. predict an energy difference between the cis and trans structures of 3.3 kcal mol^{-1} at the UHF/6-31G* level; they also predict C–O bond dissociation energies of 33.0 kcal mol^{-1} at the MP3/6-31G*//HF/6-31G* level and 28.9 kcal mol^{-1} at the MP2/6-311G**//HF/6-31G* level of theory. The latter compares favorably with the experimental values of 33.3[18] or 34.9 kcal mol^{-1} [21] for this bond energy. Charge distribution analysis of the wave functions shows that there is a greater negative charge on the inner oxygen atom; however, the spin density is exclusively on the terminal oxygen. These arguments are consistent with electronegativity and Lewis structure arguments.

It has been argued[28] that further progress in the understanding of the reaction mechanism will not be possible without a comprehensive ab initio quantum mechanical investigation. In that vein we have applied ab initio techniques to aspects of the reaction. In this first paper we study the conformers of the ethylperoxy radical ($C_2H_5O_2^\bullet$) in terms of energies and interconversions between various forms. In subsequent articles we intend to investigate other areas of the $C_2H_5^\bullet + O_2$ reaction surface.

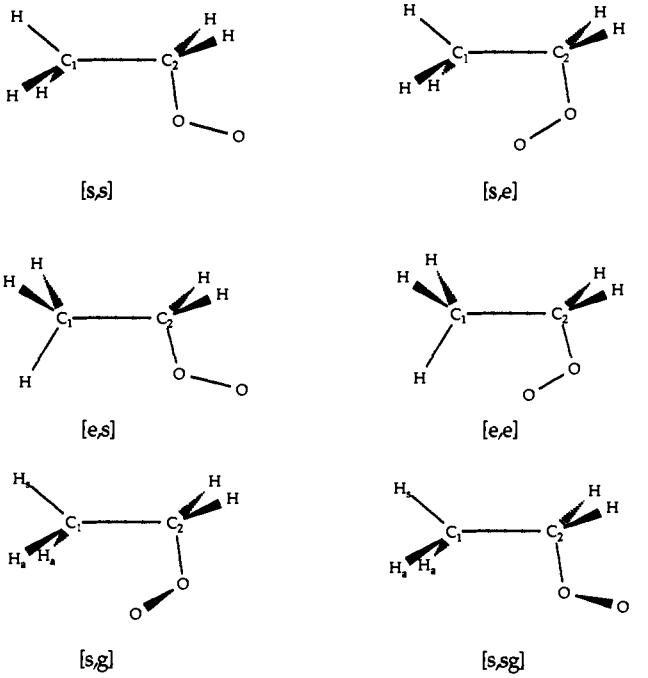

Figure 2. Definitions of the nomenclature used in this study for the ethylperoxy radical.

III. Computational Methods

Ab initio theoretical studies at various levels of theory have been performed on six conformers of the $^2A''$ state and four conformers of the $^2A'$ state. Structures of the conformers of the ethylperoxy radical are shown in Figure 2. In addition, studies were performed on the reactants, $C_2H_5^\bullet + O_2$, for purposes of comparison. Three Gaussian-type orbital basis sets have been used. The smallest basis used was the STO-3G of Hehre, Stewart, and Pople.[62] The second basis was the standard double-zeta (DZ) set of Huzinaga[63] and Dunning,[64] designed C, O(9s5p/4s2p), H(4s/2s). The largest basis was the double-zeta plus polarization (DZP) set, constructed by appending a set of six d-like functions to each carbon ($\alpha_d = 0.75$) and oxygen ($\alpha_d = 0.85$) atom and a set of p functions to hydrogen ($\alpha_p = 0.75$) to the DZ basis described above. The number of basis functions resulting was 25 for the STO-3G basis, 50 for DZ, and 89 for DZP.

Restricted open-shell Hartree–Fock theory[65] was used for all studies. Optimized geometries were obtained using analytic SCF first derivatives.[66] Harmonic vibrational frequencies were evaluated at SCF

(45) Bennett, J. E.; Summers, R. *J. Chem. Soc., Faraday Trans. 2* **1973**, *69*, 1043.
(46) Kemp, T. J.; Welbourn, M. *Tetrahedron Lett.* **1974**, 87.
(47) Chamulitrat, W.; Takahashi, N.; Mason, R. P. *J. Biol. Chem.* **1989**, *264*, 7889.
(48) Mihelcic, D.; Volz-Thomas, A.; Paetz, H. W.; Kley, D.; Mihelcic, M. *J. Atmos. Chem.* **1990**, *11*, 271.
(49) Parkes, D. A.; Paul, D. M.; Quinn, C. P.; Robson, R. C. *Chem. Phys. Lett.* **1973**, *23*, 425.
(50) Munk, J.; Pagsburg, P.; Ratajczak, E.; Sillesen, A. *J. Phys. Chem.* **1986**, *90*, 2752.
(51) Cattell, F. C.; Cavanagh, J.; Cox, R. A.; Jenkin, M. E. *J. Chem. Soc., Faraday Trans. 2* **1986**, *82*, 1999.
(52) Wallington, T. J.; Dagaut, P.; Kurylo, M. J. *J. Photochem. Photobiol.* **1988**, *42*, 173.
(53) Niki, H.; Maker, P. D.; Savage, C. M.; Breitenbach, L. P. *J. Phys. Chem.* **1982**, *86*, 3825.
(54) Wallington, T. J.; Gierczak, C. A.; Ball, J. C.; Japar, S. M. *Int. J. Chem. Kinet.* **1989**, *21*, 1077.
(55) Anastasi, C.; Waddington, D. J.; Woolley, A. *J. Chem. Soc., Faraday Trans. 1* **1983**, *79*, 505.
(56) Biskupic, S.; Valko, L. *J. Mol. Struct.* **1975**, *27*, 97.
(57) Ohkubo, K.; Kitagawa, F. *Bull. Chem. Soc. Jpn.* **1975**, *48*, 703.
(58) Kucher, R. V.; Opeida, I. A.; Dmitruk, A. F.; Kholoimova, L. I. *Oxid. Commun.* **1983**, *5*, 75.
(59) Ohkubo, K.; Fujita, T.; Sato, H. *J. Mol. Struct.* **1977**, *36*, 101.
(60) Skancke, A.; Skancke, P. N. *J. Mol. Struct. (THEOCHEM)* **1990**, *207*, 201.
(61) Boyd, S. L.; Boyd, R. J.; Barclay, L. R. C. *J. Am. Chem. Soc.* **1990**, *112*, 5724.
(62) Hehre, W. J.; Stewart, R. F.; Pople, J. A. *J. Chem. Phys.* **1969**, *51*, 2657.
(63) Huzinaga, S. *J. Chem. Phys.* **1965**, *42*, 1293.
(64) Dunning, T. H. *J. Chem. Phys.* **1970**, *53*, 2823.
(65) Roothaan, C. C. J. *Rev. Mod. Phys.* **1960**, *32*, 179.
(66) (a) Pulay, P. In *Modern Theoretical Chemistry*; Schaefer, H. F., Ed.; Plenum: New York, 1977. (b) Goddard, J. D.; Handy, N. C.; Schaefer, H. F. *J. Chem. Phys.* **1979**, *71*, 1525.

Table II. Selected Geometric Parameters (Å and deg) for the $^2A''$ State of the Ethylperoxy Radical at the CISD Level of Theory[a]

	[s,s]		[s,e]		[e,s]		[e,e]		[s,g]		[s,sg]		reactants	
	DZ	DZP	DZ	DZP	DZ	DZP	DZ	DZP	DZ	DZP	DZ	DZP	DZ	DZP
r(CC)	1.535	1.514	1.538	1.513	1.546	1.527	1.549	1.526	1.538	1.516	1.537	1.516	1.522	1.498
r(CO)	1.496	1.440	1.508	1.451	1.500	1.444	1.519	1.461	1.496	1.440	1.499	1.444		
r(OO)	1.393	1.312	1.384	1.306	1.391	1.310	1.378	1.302	1.393	1.312	1.389	1.310	1.203	1.202
oop(C_2)	−37.2	−36.2	−41.2	−39.8	−37.9	−36.9	−42.9	−41.3					9.9	2.8
θ(CCO)	106.0	107.1	114.5	115.0	105.9	107.2	115.8	116.4	111.2	111.6	108.4	109.2		
θ(COO)	110.8	110.7	114.4	114.2	111.0	110.7	116.1	116.0	110.9	110.7	112.0	112.1		

[a] Nomenclature is described in the text. The reactants are $C_2H_5^{\bullet}$ and O_2.

Table III. Selected Geometric Parameters (Å and deg) for the $^2A'$ State of the Ethylperoxy Radical at the SCF Level of Theory[a]

	[s,s]		[s,e]		[e,s]		[e,e]	
	DZ	DZP	DZ	DZP	DZ	DZP	DZ	DZP
r(CC)	1.521	1.517	1.528	1.522	1.532	1.531	1.542	1.539
r(CO)	1.461	1.418	1.476	1.434	1.464	1.420	1.480	1.437
r(OO)	1.419	1.359	1.418	1.360	1.418	1.359	1.416	1.358
oop(C_1)	31.0	31.0	31.4	31.4	31.6	31.6	−32.3	−32.3
oop(C_2)	36.1	34.9	40.3	38.7	36.8	35.5	41.4	39.7
θ(CCO)	106.3	107.1	114.9	115.6	106.4	107.1	116.5	117.1
θ(COO)	108.7	107.6	113.2	112.3	108.7	107.5	114.4	113.5
Hess. index	0	0	1	1	1	1	2	2

[a] Nomenclature is described in the text. The Hessian index is the number of imaginary frequencies.

Table IV. Selected Geometric Parameters (Å and deg) for the $^2A'$ State of the Ethylperoxy Radical at the CISD Level of Theory[a]

	[s,s]		[s,e]		[e,s]		[e,e]	
	DZ	DZP	DZ	DZP	DZ	DZP	DZ	DZP
r(CC)	1.537	1.515	1.543	1.520	1.549	1.529	1.558	1.537
r(CO)	1.493	1.429	1.508	1.446	1.495	1.431	1.513	1.449
r(OO)	1.473	1.385	1.472	1.386	1.472	1.385	1.469	1.384
oop(C_1)	30.9	31.0	31.2	31.3	31.4	31.6	−32.1	−32.2
oop(C_2)	36.2	34.9	40.8	38.8	−36.8	−35.4	41.9	39.8
θ(CCO)	105.3	106.5	114.9	115.5	105.0	106.3	116.5	116.9
θ(COO)	106.8	106.4	111.4	111.3	106.9	106.3	112.5	112.4

[a] Nomenclature is described in the text.

Table V. Relative Energies (kcal mol^{-1}) of the Conformers of the Ethylperoxy Radical[a]

	DZ/SCF	DZP/SCF	DZ/CISD	DZ/CISD+Q	DZP/CISD	DZP/CISD+Q
$^2A''$ [s,s]	0.0	0.0	0.0	0.0	0.0	0.0
$^2A''$ [s,g]	0.4	0.4	0.0	−0.1	0.0	−0.1
$^2A''$ [s,sg]	1.3	1.5	0.9	0.8	1.0	0.9
$^2A''$ [s,e]	3.4	3.7	2.6	2.3	2.7	2.5
$^2A''$ [e,s]	2.6	3.0	2.4	2.3	2.9	2.7
$^2A''$ [e,e]	7.2	8.2	6.2	5.8	6.8	6.4
$^2A'$ [s,s]	9.1	12.2	12.3	13.5	16.3	17.4
$^2A'$ [s,e]	13.9 (4.8)	18.0 (6.2)	16.9 (4.6)	18.0 (4.5)	22.0 (5.7)	23.0 (5.6)
$^2A'$ [e,s]	11.7 (2.6)	15.2 (3.0)	14.8 (2.5)	15.9 (2.4)	19.2 (2.9)	20.2 (2.8)
$^2A'$ [e,e]	17.9 (8.8)	22.6 (10.4)	21.0 (8.7)	22.0 (8.5)	26.5 (10.2)	27.3 (9.9)
reactants	29.8	23.9	31.8	32.5	27.0	27.9

[a] Values in parentheses are relative to the [s,s] conformer of the $^2A'$ state. The values include scaled zero-point vibrational energy corrections as described in the text. The reactants are $C_2H_5^{\bullet}$ and O_2.

equilibrium geometries with the use of analytic second derivatives.[67] Infrared intensities[68] also were evaluated analytically within the double harmonic approximation. SCF level zero-point vibrational energies were scaled by a factor of 0.91.

The effects of electron correlation at the single-reference level were included by the use of configuration interaction single and double excitation (CISD) theory with the DZ and DZP basis sets. Geometry optimizations at the CISD level were performed utilizing CISD analytic gradients.[69] Corrections for the unlinked quadruple excitations in the CISD formulation (denoted by +Q in the text and tables) have been applied.[70] The active space for all CISD studies included all orbitals except the carbon and oxygen 1s; no virtual orbitals were excluded. The largest CISD optimization reported here contained 448 069 configurations in C_1 symmetry.

In order to distinguish conformers of the $C_2H_5O_2^{\bullet}$ structure, the following abbreviation will be used: [x,y], where x refers to the orientation of the CH_3 group relative to the C–O bond (either "e" for eclipsed or "s" for staggered) and y refers to the orientation around the C–O bond (either "e" for eclipsed, "g" for gauche, or "s" for staggered). In addition, in referring to the transition state between the staggered and gauche minima, the designation "sg" will be used. The designations are shown in Figure 2.

IV. Results

Geometries of all structures given in Figure 2 have been optimized at both the SCF and CISD levels of theory. Two low-lying electronic states were investigated (the molecular orbitals of which are shown in Figure 3), namely, $^2A''$ and $^2A'$. For the [s,g] and [s,sg] structures (C_1 symmetry), only the ^2A state (corresponding

(67) Pople, J. A.; Krishnan, R.; Schlegel, H. B.; Binkley, J. S. *Int. J. Quant. Chem.* **1979**, *S13*, 225.

(68) Yamaguchi, Y.; Frisch, M. J.; Gaw, J. F.; Schaefer, H. F.; Binkley, J. S. *J. Chem. Phys.* **1986**, *84*, 2262.

(69) Brooks, B. R.; Laidig, W. D.; Saxe, P.; Goddard, J. D.; Yamaguchi, Y.; Schaefer, H. F. *J. Chem. Phys.* **1980**, *72*, 4652. Rice, J. E.; Amos, R. D.; Handy, N. C.; Lee, T. J.; Schaefer, H. F. *J. Chem. Phys.* **1986**, *85*, 963. Osamura, Y.; Yamaguchi, Y.; Schaefer, H. F. *J. Chem. Phys.* **1981**, *75*, 2919. Osamura, Y.; Yamaguchi, Y.; Schaefer, H. F. *J. Chem. Phys.* **1982**, *77*, 383.

(70) Langhoff, S. R.; Davidson, E. R. *Int. J. Quant. Chem.* **1974**, *8*, 61.

Table VI. Vibrational Frequencies Predicted for the Ethyl Radical and Oxygen Molecules in This Work (at the DZP/SCF Level), Compared to Experimental and Previous Theoretical Work[a]

	this work			previous work		
	unscaled	scaled	sym	*b*	*c*	assignment
ω_1	3403	3097	a″	3112	3114	asym CH_2 stretch
ω_2	3300	3003	a′	3033	3036	sym CH_2 stretch
ω_3	3259	2966	a″	2987	2987	asym CH_3 stretch
ω_4	3227	2937	a′	2920	2920	sym CH_3 stretch
ω_5	3162	2877	a′	2842	2844	sym CH_3 stretch
ω_6	1604	1460	a″	1440	1442	CH_3 internal bend
ω_7	1603	1459	a′	1439	1442	CH_3 internal bend
ω_8	1590	1447	a′		1383	CH_2 scissor
ω_9	1523	1386	a′	1366	1369	CH_3 internal bend
ω_{10}	1296	1179	a′	1138	1133	CH_3 rock
ω_{11}	1115	1014	a″	1175	1185	C–C stretch
ω_{12}	1070	974	a′		1025	CH_3 rock
ω_{13}	860	783	a″			CH_2 asym bend
ω_{14}	517	470	a′	540	532	CH_2 pyramidal
ω_{15}	196	178	a″			CH_2 torsion
	2024	1842				O–O stretch in O_2

[a] The scaling factor used was 0.91. [b] Experimental and theoretical: Pacansky, J.; Dupuis, M. *J. Am. Chem. Soc.* **1982**, *104*, 415. [c] Experimental work: Chettur, G.; Snelson, A. *J. Phys. Chem.* **1987**, *91*, 3483.

Table VII. Vibrational Frequencies Predicted for the Ethylperoxy Radical (at the DZP/SCF Level), Compared to Experimental and Previous Theoretical Work[a]

	this work			previous work		
	$^2A''$	$^2A'$	sym	*b*	*c*	assignment
ω_1	2997	2961	a″	3016	2955	asym CH_2 stretch + CH_3 asym stretch
ω_2	2983	2985	a′		2936	sym CH_3 stretch
ω_3	2977	2995	a″			asym CH_3 stretch − CH_2 asym stretch
ω_4	2938	2921	a′		2901	sym CH_2 stretch
ω_5	2911	2913	a′		2874	sym CH_3 stretch
ω_6	1500	1508	a′	1474	1493	CH_2 scissor
ω_7	1472	1473	a′	1451	1467	CH_3 internal bend
ω_8	1456	1456	a″	1389	1454	CH_3 o.p. bend
ω_9	1423	1423	a′	1351	1371	CH_2 wag
ω_{10}	1377	1380	a′	1380	1410	CH_3 sym bend
ω_{11}	1271	1271	a″	1242	1259	CH_2 twist
ω_{12}	1180	1113	a′	1112	1145	O–O stretch
ω_{13}	1163	1172	a″		1152	CH_3 o.p. rock
ω_{14}	1145	1131	a′	1136	1129	CH_3 i.p. rock
ω_{15}	1032	1026	a′	1009	1006	C–C stretch
ω_{16}	873	869	a′	838	859	C–O stretch
ω_{17}	795	811	a″	800	786	CH_2 rock
ω_{18}	498	448	a′	499	491	COO bend
ω_{19}	306	291	a′		300	CCO bend
ω_{20}	235	234	a″			τ(HCCO)
ω_{21}	102	121	a″			τ(CCOO)

[a] The frequencies for this work have been scaled by 0.91. [b] Experimental: Chettur, G.; Snelson, A. *J. Phys. Chem.* **1987**, *91*, 3483. [c] Theoretical: Wagner, A. F.; Melius, C. Unpublished results.

to the $^2A''$ state in C_s symmetry) was studied. Selected geometrical parameters for the $^2A''$ state are given in Tables I (SCF) and II (CISD) with results for the $^2A'$ state in Tables III (SCF) and IV (CISD). Tables I and III contain a row labeled "Hessian Index"; this is the number of imaginary frequencies predicted for each system at the SCF level. Table V shows the relative energies of all species at all levels of theory used; the relative energies include corrections due to the zero-point vibrational energy as described in the Computational Methods section. In addition, Table V contains relative energy values for the reactants ($C_2H_5^\bullet + O_2$). Values for the reactants at the CISD level were obtained by study of the "supermolecule", i.e., the $C_2H_5^\bullet$ and O_2 moieties were separated by 200 Å. Table VI includes a comparison between our evaluated frequencies for the ethyl radical and values obtained previously from theoretical and experimental methods. Table VII incorporates a similar comparison for the ethylperoxy radical.

Tables 8–29 (supplementary material) contain complete geometries, total energies, and vibrational frequencies for all structures (including reactants) discussed in this paper.

V. Discussion

(a) Molecular Geometries. Turning first to the $^2A''$ state, at the SCF level we notice a consistent reduction in bond length in moving from the DZ to DZP results, as expected. This change is smallest for C–C, larger for C–O, and largest for the O–O bond, where a reduction of ≈0.06 Å is observed. The C–C bond is somewhat shorter than the typical C–C single bond of 1.54 Å[71] but is longer than the C–C bond in the ethyl radical at the same level of theory (Table I). The C–O bond length lies within the usual range for C–O single bonds[72] with the O–O distance lying between typical values for single and double O–O linkages, i.e., 1.48 and 1.21 Å, respectively.[71] The theoretically predicted values for O_2 itself are 1.166 (DZP/SCF) and 1.202 Å (DZP/CISD), the latter being close to the experimental value of 1.208 Å.[72]

For geometries at the CISD level, similar arguments can be made, although the bond lengths are uniformly longer due to the effects of electron correlation. In all cases, the values for angles are essentially unchanged to within 5°.

Turning to the $^2A'$ state, all of the above arguments hold. Increasing the basis set size at SCF and CISD levels decreases the bond lengths of C–C by a small amount, C–O by a greater

(71) Elmsley, J. *The Elements*; Clarendon: Oxford, 1989.
(72) *Handbook of Chemistry and Physics*, 71st ed.; Lide, D. R., Ed.; CRC: Boca Raton, FL, 1990.

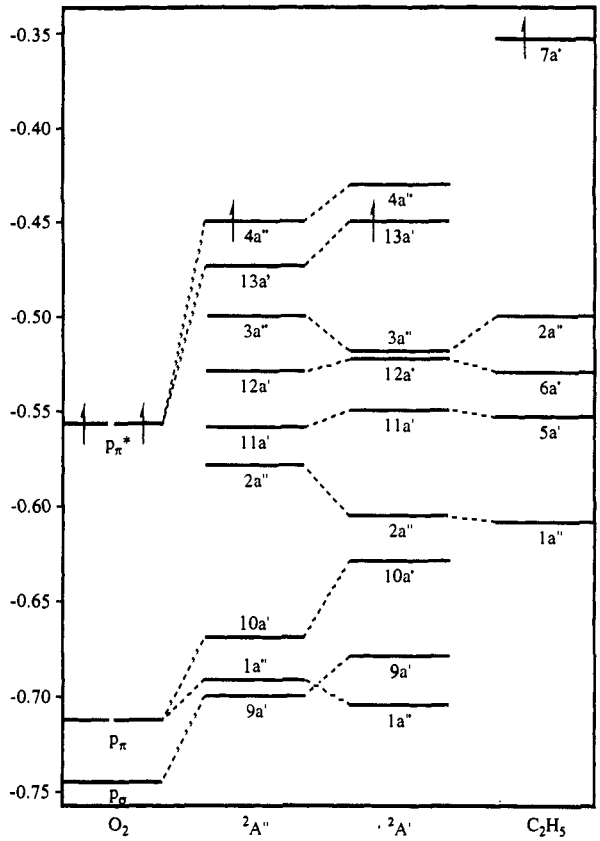

Figure 3. Orbital interaction diagram for the [s,s] isomers of the ethylperoxy radical in the $^2A''$ and $^2A'$ states. Orbital energies are in a.u. All orbitals (except those marked) are doubly occupied.

amount, and O–O by a wide margin. The CISD bond lengths are greater than the corresponding values at the SCF level but again decrease with the addition of polarization functions. Angles change by small amounts for this state as well.

Comparison of the same conformers for both $^2A''$ and $^2A'$ states reveals clearly that the major changes on excitation are restricted to the increase of the O–O bond length by ≈0.05 Å and a concomitant decrease in the C–O–O angle.

In order to understand the differences, we have analyzed the MOs of the [s,s] conformers of the two states. The same qualitative arguments may be used on the other conformers. For the $^2A''$ state the electronic configuration is (DZP/SCF results):

$$[1\text{–}9]a'^2\ 1a''^2\ 10a'^2\ 2a''^2\ 11a'^2\ 12a'^2\ 3a''^2\ 13a'^2\ 4a''$$

and the $^2A'$ state:

$$[1\text{–}8]a'^2\ 1a''^2\ 9a'^2\ 10a'^2\ 2a''^2\ 11a'^2\ 12a'^2\ 3a''^2\ 4a''^2\ 13a'$$

The valence region is comprised essentially of the highest eight doubly occupied MOs (DOMOs) and the singly occupied MO (SOMO). If we analyze the SOMO first, we find, in agreement with previous work,[61] that for the $^2A''$ state the electron resides in an O_2-like out-of-plane (oop) π^* orbital. This is to be expected, as this is one "half" of the π^* orbital of diatomic O_2. For the $^2A'$ state the single electron resides in a p-like orbital on the terminal O atom, in a direction perpendicular to the O–O bond in the plane; this is clearly derived from the other "half" of the π^* orbital of O_2 mentioned above.

Figure 3 contains an MO interaction diagram that summarizes the valence orbitals of the reactants, $C_2H_5^\bullet$ and O_2, and the two states of interest for the ethylperoxy radical. At first glance the figure looks relatively straightforward. The O_2 possesses p_σ and p_π filled orbitals, with the p_{π^*} being half-filled, resulting in the observed triplet state. The ethyl radical has a C–C bonding orbital, C–H bonding orbitals, and the radical orbital, the latter of which is essentially a 2p orbital on the CH_2 center. (The energy levels of the SOMOs are arbitrary.)

The formation of either of the $^2A''$ or $^2A'$ states would initially be assumed to arise simply from the interaction of the C2p radical orbital with either of the π^* components of O_2. For the $^2A''$ since the radical orbital interacts with the in-plane π^* orbital on O_2; this increases the O–O distance by increasing the electron population in an antibonding orbital, leaving one electron in the oop π^* component. The remaining orbitals deriving from the ethyl radical are essentially unchanged in the ethylperoxy radical; the 2a″ orbital is raised somewhat in energy possibly as a reaction to the rise in the O_2-like 1a″ orbital. For the $^2A''$ orbitals deriving from O_2, a significant increase in energy is observed, due most probably to the increased O–O bond length discussed previously.

Moving to the $^2A'$ state we see a significant difference from the orbitals of the $^2A''$ state, militating against the simple interpretation of the interaction given above. The O_2–like π^* orbitals are higher in energy due to the population of the oop π^* fragment orbital. This results in a gradual lengthening of the O–O bond from 1.199 Å in O_2 to 1.367 Å in the $^2A''$ state of the ethylperoxy radical to 1.419 Å in the $^2A'$ state (Tables I and III). The lower O_2-like orbitals—9a′ and 10a′ and 1a″—all have changed significantly from their position in the $^2A''$ state. All these levels have shifted higher except for the 1a″, which has lowered significantly and has, in fact, crossed over to below the 9a′ level. The ethyl radical-like orbitals also have moved to a significant degree.

At first sight, as discussed above, it would appear that the C–O bond formed from the interaction of the $C_2H_5^\bullet$ and O_2 fragments would result from the interaction of the radical orbital on $C_2H_5^\bullet$ and the π^* orbitals on O_2. However, on analysis, this interpretation is somewhat simplistic. First, we note that there is no significant difference between the $^2A''$ and $^2A'$ states for the C–O bond length. Second, the manifold of orbitals has changed significantly between the two states. Third, this simplistic argument does not allow a strong bond to form in the $^2A'$ state at all since the radical orbital on $C_2H_5^\bullet$ is of a′ symmetry. Interaction with the a″ component on the O_2 π^* is therefore forbidden, resulting in no net bonding since the overall state must be A′. Therefore, it would appear that the C–O binding must be manifest in other MOs. Indeed, for the $^2A''$ state the C–O bond has components in the 9a′ and 13a′ orbitals, whereas for the $^2A'$ state it occurs to any great extent only in the 9a′ orbital. The latter observation, however, leads to the conclusion that the $^2A'$ state of the ethylperoxy radical is derived from an excited state of either $C_2H_5^\bullet$ or O_2. Based on experimental and theoretical work discussed earlier,[39–41] $C_2H_5^\bullet$ seems an unlikely candidate. However, the lowest excited state of O_2 is the $^1\Delta_g$ state at 0.98 eV (22.6 kcal mol^{-1}).[73] This state can result in an attractive interaction in the $^2A'$ state of the ethylperoxy radical. The energy difference of the excited state compares favorably with the adiabatic energy difference between the $^2A''$ and $^2A'$ states of 12.2 kcal mol^{-1} (DZP/SCF), allowing for the inevitable orbital relaxation.

(b) Vibrational Frequencies. Although there are few experimental data on the vibrational frequencies of the ethyl and ethylperoxy radicals, we shall nevertheless attempt to correlate our results with them. The comparisons are summarized in Table VI for the ethyl radical and Table VII for the ethylperoxy radical. Turning first to the ethyl radical, there are two sets of experimental data to compare, yielding good agreement. The only difficulty in assignment concerns the CH_3 rocking mode and the C–C stretch. Our scaled value for the rock agrees well with the experimental assignment of the stretch; however, both experiments give similar values for this mode, although the difference is greater than that observed for other modes. In the theoretical work of Pacansky and Dupuis,[36] the authors report a value of 1096 cm^{-1} for the C–C stretch, which is in good agreement with our unscaled value when taking into account the larger basis used here. In addition, the previous work puts both CH_3 rocking modes *above* the C–C stretch. Therefore, we suggest that the experimental value of 1025 cm^{-1} corresponds to the C–C stretch, with the 1175

(73) Herzberg, G. *Molecular Spectra and Molecular Structure. I. Spectra of Diatomic Molecules*, 2nd ed.; Van Nostrand: New York, 1950; Chapter 6.

and 1185 cm^{-1} values being the CH_3 rock. This leaves the 1138–1133 cm^{-1} bands found experimentally, unassigned, with no clear choices for $C_2H_5^{\bullet}$. We note that the discrepancies between theory and experiment for all other modes (except as noted below) are less than 40 cm^{-1}, which would be the minimum necessary for assignment to any of our scaled values. The 1138 cm^{-1} absorption, interestingly, has no isotopically substituted analogues; also, Pacansky and Dupuis state that "...1175 and 1138 cm^{-1} in $CH_3CH_2^{\bullet}$ could be assigned to either C–C stretch or rocking motion of the CH_3 group". The authors further state that they prefer 1175 cm^{-1} as the rock and 1138 cm^{-1} as the stretch since the stretch should be affected less dramatically by deuteration. However, as noted above, the 1138 cm^{-1} mode has not been observed in any of the deuteration experiments.

It is no surprise that the predicted value for the CH_2 wag mode is poorly reproduced from the theoretical studies as compared to the experimental result; this mode is undoubtedly highly anharmonic and thus is difficult to reproduce accurately.

The assignments of the vibrational frequencies for the ethylperoxy radical (Table VII) produce some interesting observations. Although the majority of frequencies agree well between the two electronic states (mirroring the closeness of the geometries discussed above), there are a few differences in assignment. As would be expected, the largest difference is for the O–O stretch. The frequency for this mode is 1180 cm^{-1} in the $^2A''$ state and 1113 cm^{-1} in the $^2A'$ state. Concomitant with this is the change in the C–O–O deformation frequency from 498 cm^{-1} to 448 cm^{-1} in the $^2A''$ and $^2A'$ states, respectively. Between the two states the asymmetric CH_2 stretch and the asymmetric CH_3 stretch modes are swapped; however, the actual situation is more complex than this since in the $^2A''$ state the frequencies are almost a 50% mix of the two modes, with the assignment in Table VII indicating the largest component first. For $^2A'$, however, the two modes are almost exclusively the first over the second component.

Comparison of our assignments with those published previously again indicates some disagreement, and once more this is less significant than might be assumed at first glance. The largest discrepancy occurs in the assignment of the CH_3 oop bend, which is in error by almost 70 cm^{-1}. It appears that the experimental spectrum has two modes near 1380 cm^{-1} (i.e., 1380 and 1389 cm^{-1}); however, both theoretical spectra (after scaling) are inconsistent with this. It is possible that the molecule is trapped in two distinct matrix sites, hence giving two frequencies for the same mode.

A more troublesome assignment is the CH_2 wag. Our assignment shows that the CH_2 wag and the CH_3 symmetric bend are strongly mixed. This would be expected, since they are similar in value and have the same symmetry, and consequently a small change in the potential surface could lead to the alternative (switched) assignment. In addition, it is unclear how anharmonicity, an effect that is neglected in the theoretical treatment, may affect the ordering. A further consequence is that if the experimental values 1474 (CH_2 scissor) and 1451 cm^{-1} (CH_3 internal bend) were reassigned to the CH_3 internal bend and the CH_3 oop bend, respectively, then a much closer agreement with both theoretical studies is achieved.

It is interesting to note that the experimental value for the O–O stretch, 1112 cm^{-1}, lies extremely close to the theoretical value for the excited $^2A'$ state. Thus it is conceivable that the experiment has measured this state in addition to the ground $^2A''$ state.

(c) Energetics and Implications for Kinetics Modelling. Relative energies for all species studied here (relative to the $^2A''$ [s,s] conformer) are given in Table V, with values relative to $^2A'$ [s,s] in parentheses. It is noted that the [s,s] and [s,g] conformers have almost the same energy. This is attributed to the size of the H atom, giving essentially no interaction between the terminal oxygen and the methylene hydrogen atom gauche to it. The barrier to rotation about the C–C bond is given by the [e,s] line for both states and is consistent between levels of theory at ≈2.5–3.0 kcal mol^{-1}. For comparison, the barrier to rotation about the C–C bond in ethane is ≈3.0 kcal mol^{-1}.[74] This agreement between the two states is a consequence of the fact that the ethyl moiety geometries are highly similar in the two electronic states.

The barrier to eclipsing of the terminal oxygen atom with the methyl carbon atom gives a barrier of ≈2.5 kcal mol^{-1} for the $^2A''$ state and ≈5.6 kcal mol^{-1} for the $^2A'$ state. The most logical explanation is that since the O–O bond is much longer in the excited $^2A'$ state, as discussed above, the terminal oxygen atom and methyl carbon come into closer proximity in the [s,e] conformer of $^2A'$ than in the analogous conformer of the $^2A''$ state. The precise values for these barriers are essential for the kinetic models. The crucial point on the surface, as discussed above, is the ring transition state. To form this state, the ethylperoxy radical must rotate around the C–C and C–O bonds such that a methyl H and the terminal O atom are close enough to begin interacting. The transition state is essentially that for an intramolecular hydrogen transfer reaction.

In the RRKM modelling work of Wagner et al.,[28] the two internal rotations were represented by harmonic torsional potentials. The authors performed some test calculations using a hindered rotor and a harmonic potential. The results showed little effect on the overall reaction. Our studies have demonstrated that the gauche and staggered conformers are isoenergetic, providing good confirmation of the validity of this part of the RRKM model.

In comparison with experimental values, our results, while not extremely accurate, are encouraging. As discussed in the Introduction, the experimental bond dissociation energy of C–O in the ethylperoxy has been reported as 33.3 or 34.9 kcal mol^{-1}. Wagner et al. quote a value for ΔH°_0 of 32.9 kcal mol^{-1}, which is directly comparable to our values given in Table V. Our best value for the bond energy is 27.9 kcal mol^{-1} (DZP/CISD+Q); the difference is of the order of our estimated error bars of ±5 kcal mol^{-1}, which one would expect from studies at this level of theory. Indeed, Boyd et al.[61] show that, with MP3/6-31G**//HF/6-31G* level studies, good agreement with experiment can be attained. However, even with this level of theory, fortuitous agreement may be occurring as is well demonstrated by our DZ/CISD results. The errors in our work are due to the fact that the reactants contain one fewer bond than the ethylperoxy radical, and hence will, to a first approximation, be better described with the CISD level of theory.

VI. Conclusions

In this work we have investigated aspects of the reaction mechanism of ethane combustion. An important part of the mechanism is the energy required to interconvert conformers of the ethylperoxy radical. This radical is formed directly from the reactants, $C_2H_5^{\bullet} + O_2$, and goes on to form the important ring transition state which is the rate-limiting step for the reaction. We have evaluated barriers to interconversion for this species consistent with the RRKM model of Wagner et al.[28]

We have assigned the IR spectra for the ethyl and ethylperoxy radicals and compared our assignments with those made previously by theoretical and experimental methods. In both cases we have suggested slightly modified assignments. Further work will be needed to confirm our assignments.

One point that to our knowledge has not been touched upon previously is that there are two states of interest for the ethylperoxy radical, namely, a $^2A''$ ground state and a $^2A'$ excited state. We have discussed the origin of both states in relation to the reactant species, $C_2H_5^{\bullet} + O_2$. We believe that the $^2A'$ state (17.4 kcal mol^{-1} above $^2A''$ at the DZP/CISD+Q level) is derived from the first excited state of O_2 ($^1\Delta_g$) which occurs at 22.6 kcal mol^{-1} above the ground $^3\Sigma_g^-$ state.

We also present results of the first study of the gauche structure for $C_2H_5O_2^{\bullet}$. This conformer is essentially isoenergetic with the staggered species, confirming that the harmonic torsional model used in kinetic modelling work is based on firm foundations. The barrier to interconversion between the staggered and gauche forms is only about 1 kcal mol^{-1}.

(74) Streitweiser, A.; Heathcock, C. H. *Introduction to Organic Chemistry*, 3rd ed.; Macmillan: New York, 1985; Chapter 5.

Subsequent work will investigate the ring transition state and the species resulting from its decomposition.

Acknowledgment. We thank Dr. Albert F. Wagner (Argonne National Laboratory) for drawing our attention to the C_2H_5 + O_2 reaction in the course of two lectures at the Center for Computational Quantum Chemistry. We also thank Dr. Les Batt (University of Aberdeen, Scotland) for many helpful discussions. This research was supported by the U.S. Department of Energy, Office of Basic Energy Sciences, Division of Chemical Sciences, Fundamental Interactions Branch, Grant No. DE-FG09-87ER13811.

Registry No. $C_2H_5O_2$, 3170-61-4; C_2H_5, 2025-56-1; O_2, 7782-44-7; C_2H_6, 74-84-0.

Supplementary Material Available: Tables 8-29 containing complete geometries, total energies, and vibrational frequencies for all structures (including reactants) discussed in this paper (33 pages). Ordering information is given on any current masthead page.

Proton Affinity of Methyl Nitrate: Less than Proton Affinity of Nitric Acid

Timothy J. Lee*,† and Julia E. Rice*,‡

Contribution from the NASA Ames Research Center, Moffett Field, California 94035, and IBM Research Division, Almaden Research Center, San Jose, California 95120.
Received February 10, 1992

Abstract: The equilibrium structures, dipole moments, harmonic vibrational frequencies, and infrared intensities of methyl nitrate, methanol, and ten structures of protonated methyl nitrate have been investigated using state-of-the-art ab initio quantum mechanical methods. The ab initio methods include self-consistent field (SCF), second-order Møller-Plesset (MP2) perturbation theory, single- and double-excitation coupled-cluster (CCSD) theory, and the CCSD(T) method, which incorporates a perturbational estimate of the effects of connected triple excitations. The MP2 equilibrium geometry and vibrational frequencies of methyl nitrate and methanol are in good agreement with experiment. The lowest energy gas-phase form of protonated methyl nitrate is a complex between methanol and NO_2^+, although the next lowest isomer is only 4.9 kcal/mol higher in energy. The $CH_3OH\cdots NO_2^+$ complex is bound by 19.6 ± 2 kcal/mol. The ab initio proton affinity (PA) of methyl nitrate is 176.9 ± 5 kcal/mol, in very good agreement with the experimental value of 176 kcal/mol. The results of this study are contrasted with an earlier study on protonated nitric acid, and it is shown that methyl nitrate possesses a *smaller* PA than nitric acid. An explanation for this phenomenon is presented.

1. Introduction

The proton affinity (PA) of nitric acid (HNO_3) has been the subject of two recent experimental papers[1,2] and a recent ab initio study.[3] The experimental data were interpreted to yield a PA for HNO_3 of 168 ± 3 kcal/mol, while the high-level ab initio study obtained a value of 182.5 ± 4.0 kcal/mol; clearly a discrepancy exists between theory and experiment. The experimental[4] PA of methyl nitrate, CH_3NO_3, would appear to support the experimental determination of the PA of nitric acid. That is, the experimental PA of methyl nitrate (176 kcal/mol[4]) is about 8 kcal/mol larger than the experimental PA of nitric acid, which is consistent with the general observation that the molecule HOA has an 8-15 kcal/mol smaller PA than the analogous CH_3OA molecule. For example, the PAs of H_2O and CH_3OH are 166 and 182 kcal/mol,[5] respectively. The larger PA of CH_3OA relative to HOA is due to the better σ electron donating ability of CH_3 relative to H.

As has been discussed in detail,[1-3,6] the most stable form of protonated nitric acid is a complex between H_2O and NO_2^+. By analogy it is expected that a complex between CH_3OH and NO_2^+ will, at the very least, be a low-lying isomer of protonated methyl nitrate. There is also experimental evidence for the existence of two distinct isomers of protonated methyl nitrate.[4,7] Hence it is certain that several structures of protonated methyl nitrate must be investigated in order to determine the most stable form. This task is further complicated by the various isomers that exist due to internal rotation of the methyl group and also those due to internal rotation of the NO_2 group. However, it is possible to restrict the number of important structures of CH_3NO_3 and $CH_3NO_3H^+$ to those with a planar NO_3 group. Smith and Marsden[8] have recently studied several forms of methyl nitrate and they found, consistent with nitric acid,[3,6] that the lowest energy forms of methyl nitrate always have a planar NO_3 moiety. Forms in which NO_3 is nonplanar are 6-9 kcal/mol higher in energy. Even with this restriction to molecules with planar NO_3 groups, we have identified ten different structures of protonated methyl nitrate.

Protonated methyl nitrate has been previously examined at the self-consistent field (SCF) level of theory using the STO-3G and 4-31G basis sets.[9] In that study only two isomers of $CH_3NO_3H^+$ were considered—one corresponding to a complex between CH_3OH and NO_2^+ and one corresponding to protonation of the nitro group. Using the 4-31G basis set, Bernardi et al.[9] found that the isomer arising from protonation of the nitro group was 6.7 kcal/mol more stable than the complex. However, given the

† NASA Ames Research Center.
‡ IBM Research Division, Almaden Research Center.

(1) Cacace, F.; Attina, M.; de Petris, G.; Speranza, M. *J. Am. Chem. Soc.* **1989**, *111*, 5481.
(2) Cacace, F.; Attina, M.; de Petris, G.; Speranza, M. *J. Am. Chem. Soc.* **1990**, *112*, 1014.
(3) Lee, T. J.; Rice, J. E. *J. Phys. Chem.* **1992**, *96*, 650.
(4) Attina, M.; Cacace, F.; Yanez, M. *J. Am. Chem. Soc.* **1987**, *109*, 5092.
(5) Lias, S. G.; Liebman, J. F.; Levin, R. D. *J. Phys. Chem. Ref. Data* **1984**, *13*, 695.
(6) Nguyen, M.-T.; Hegarty, A. F. *J. Chem. Soc., Perkin Trans. 2* **1984**, 2043.
(7) de Petris, G. *Org. Mass Spectrom.* **1990**, *25*, 83.
(8) Smith, B. J.; Marsden, C. J. *J. Comput. Chem.* **1991**, *12*, 565.
(9) Bernardi, F.; Cacace, F.; Grandinetti, F. *J. Chem. Soc., Perkin Trans. 2* **1989**, 413.

0002-7863/92/1514-8247$03.00/0